*SPECIAL ISSUE ARTICLE*

# Microscale evaluation of mechanical properties of friction stir welded A6061 aluminium alloy/304 stainless steel dissimilar lap joint

**T. Ogura*[1], T. Nishida[1], Y. Tanaka[1], H. Nishida[2], S. Yoshikawa[2], M. Fujimoto[2] and A. Hirose[1]**

Microscale evaluation of the mechanical properties of a friction stir welded A6061/SUS 304 grooved lap joint was performed using a microtensile test and transmission electron microscopy. The microtensile test revealed that ~62% of the area along which the rotating tool passed the specimen was regarded as the bonded region and that the joint was fractured at the A6061 matrix owing to the formation of very thin interfacial reaction layers. Equiaxed aluminium grains were observed at the interface of the specimen after it was fractured, indicating that the interface deformed only slightly during the microtensile test. It should be noted that although the maximum tensile strength of the joint was approximately the same as that of the base alloy, the proof stress of the joint decreased with the dissolution of the $\beta''$ phase in the A6061 aluminium alloy.

**Keywords:** Friction stir welding, Dissimilar metal joint, Transmission electron microscopy, Aluminium alloys, Steels

***This paper is part of a special issue on Ecomates 2011***

## Introduction

The need for energy saving and pollution reduction has a strong impact on material selection for industries. In particular, for transportation industries, the need of the hour is to establish an effective and environmentally friendly joining technique to reduce fuel consumption by weight savings. It should be noted that the use of aluminium alloys leads to a weight reduction of component, which in turn leads to a reduction in gas emission. Therefore, it is essential to develop a joining technique that involves the use of a combination of steel and an aluminium alloy. However, a drawback of using this combination is that brittle Al rich intermetallic compounds ($Al_3Fe$ and $Al_5Fe_2$) are generally formed at the interface of aluminium alloy/steel joints owing to mutual diffusion of iron to aluminium during welding; it has been pointed out that these thicker, brittle intermetallic layers lead to a fast rupture of the joint under stress.[1–7] In order to produce a sound aluminium alloy/steel joint, it is important to reduce the welding heat input. Friction stir welding (FSW), developed by the Welding Institute (TWI),[8] has several advantages over the above-mentioned welding techniques, in that FSW has a lower welding temperature and does not lead to the formation of fusion welding defects. Therefore, FSW has the potential to be used as practical process for joining dissimilar materials. The results of our recent research reveal that a sound joint can be obtained right from the time an amorphous layer is formed owing to the mechanical alloying effects before the formation of intermetallic compounds in a friction stir welded A3003 aluminium alloy/SUS 304 stainless steel dissimilar lap joint.[9]

In general, FSW causes a severe plastic deformation and an increase in temperature within and around the stirred zone,[10] which in turn causes significant microstructural evolution including the formation of an interfacial layer and the dissolution and coarsening of precipitates. Although a number of detailed studies have been conducted on the joining of an aluminium alloy sheet to a steel sheet by FSW,[11–18] research on the microscale characterisation of the bonded region in a friction stir welded joint is essential, given the fact that the understanding of the superior part of the joint will contribute to suitable material design. In this study, therefore, microscale evaluation of the mechanical properties and interfacial microstructure of a friction stir welded A6061/SUS 304 lap joint has been carried out. For this purpose, a microtensile test, which has provided many valuable insights into the microscale mechanical properties of alloys, has been performed in combination with the transmission electron microscopy (TEM).

## Experimental

In this study, an A6061-T651 aluminium alloy plate with a thickness of 11 mm and a commercial SUS 304 plate

[1]Division of Materials and Manufacturing Science, Graduate School of Engineering, Osaka University, 2-1 Yamadaoka, Suita, Osaka 565-0871, Japan
[2]Kawasaki Heavy Industries Ltd, 3-1-1, Higashikawasaki-cho, Chuo-ku, Kobe, Hyogo 650-8670, Japan

*Corresponding author, email tomo.ogura@mapse.eng.osaka-u.ac.jp


Published by Maney on behalf of the Institute
Received 30 May 2012; accepted 4 December 2012
DOI 10.1179/1362171812Y.0000000098

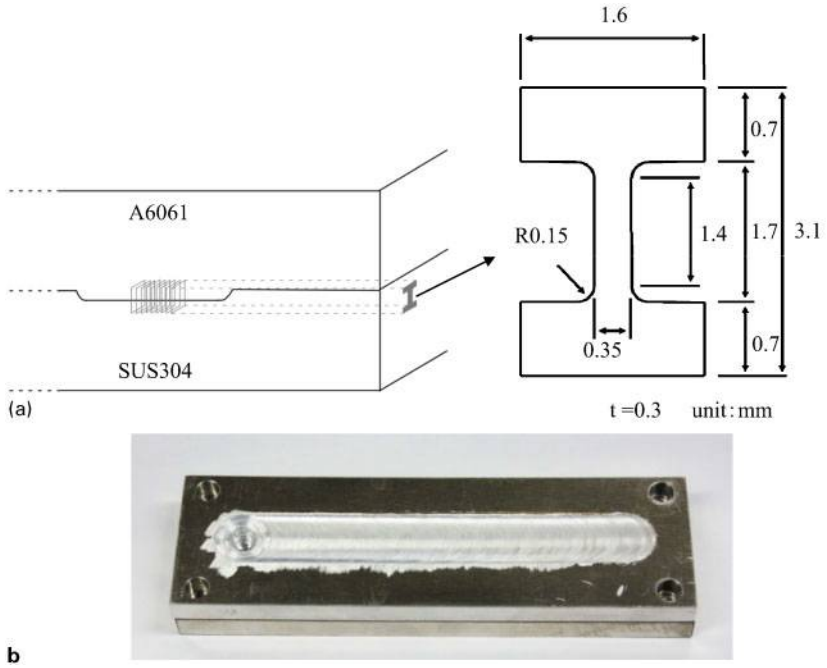


**1** ***a*** **schematic illustration of specimens used for microtensile test of friction stir welded A6061/SUS 304 grooved lap joint and** ***b*** **appearance of joint**

with a thickness of 12 mm were used. The chemical compositions of these alloys are listed in Table 1. A groove with a width of 10 mm and a depth of 0·5 mm was carved on the SUS 304 plate. This groove allows for a wide joining area and increases the strength of the joint.[19] Then, a rotating tool with a threaded probe having a diameter of 7 mm and a height of 11 mm was made of SKD series tool material. This tool was plunged from the A6061 surface onto the SUS 304 surface (plunge depth was 11·5 mm), and lap joints were produced at a rotational speed of 900 rev $min^{-1}$ and a welding speed of 300 mm $min^{-1}$. The tool was tilted at an angle of 1·5°. The top of the probe was not inserted into the steel; instead, it was placed in contact and rubbed just on the surface of SUS 304 in order to prevent pin erosion and overheating. The microVickers hardness was measured with a load of 100 g for 15 s. For microstructural analysis, cross-sectional samples were prepared using a standard metallographic procedure. The samples were then etched with Tucker's solution (HCl: 22·5%, HF: 7·5%, $HNO_3$: 7·5% and $H_2O$: bal.). Microstructural observation was carried out using a Hirox KH-7700 stereomicroscope. Transmission electron microscopy (JEM-2100F; JEOL Ltd) observation and TEM–energy dispersive X-ray (EDX) analysis were performed for the detailed analysis of the interface of the specimens that were prepared using a Hitachi FB-2000A focused ion milling (FIB). A Brother HS-300 wire cutting machine was used to prepare a specimen for the microtensile test, as shown in Fig. 1*a*. This specimen was sliced in a direction parallel to the direction of the tool axis. The dimensions of this specimen are also shown in the figure. The specimen was prepared in order to evaluate the strength in the grooved region after FSW. Figure 1*b* shows the appearance of the lap joint. This joint was successfully obtained without cracking. All tests were performed using a homemade microtensile testing machine at a constant crosshead displacement rate of 1·0 μm $s^{-1}$.

## Results and discussion

A standard cross-sectional image obtained after FSW is shown in Fig. 2*a*. As observed in the case of friction stir welded joints, the A6061 alloy also showed the presence of a stir zone and onion rings. It was confirmed that A6061 successfully flowed into the grooved SUS 304. Figure 2*b* shows the distribution of the microVickers hardness at the bottom of the A6061 plate. The measured hardness of the A6061 base alloy was $98{\cdot}8 \pm 1{\cdot}1$ HV. It was confirmed that the hardness along the groove decreased in comparison with that of the base alloy; this decrease is attributed to the combined effects of a decrease in hardness caused by the heat input and an increase in hardness caused by the formation of finer grains. Along the advancing side of the groove, the hardness of the A6061 alloy was ~83%, which is slightly higher than that (79%) of the A6061 alloy along the retreating side of the groove owing to larger stirring during FSW.[20,21] The hardness of the heat affected zone is ~60% that of the base alloy.

A microtensile test was performed to investigate the mechanical properties of the lap joint at each region. Figure 3 shows the maximum tensile strength at each

**Table 1 Chemical compositions of A6061 and SUS 304 plates used in this study/mass-%**

| Materials | Mg | Si | Cu | C | S | Mn | P | Ni | Cr | Fe | Al |
|---|---|---|---|---|---|---|---|---|---|---|---|
| A6061 | 1·1 | 0·66 | 0·31 | … | … | 0·07 | … | … | 0·18 | 0·37 | Balance |
| SUS 304 | … | ≤1·00 | … | ≤0·08 | ≤0·030 | ≤2·00 | ≤0·045 | 8·00–10·50 | 18·00–20·00 | Balance | … |

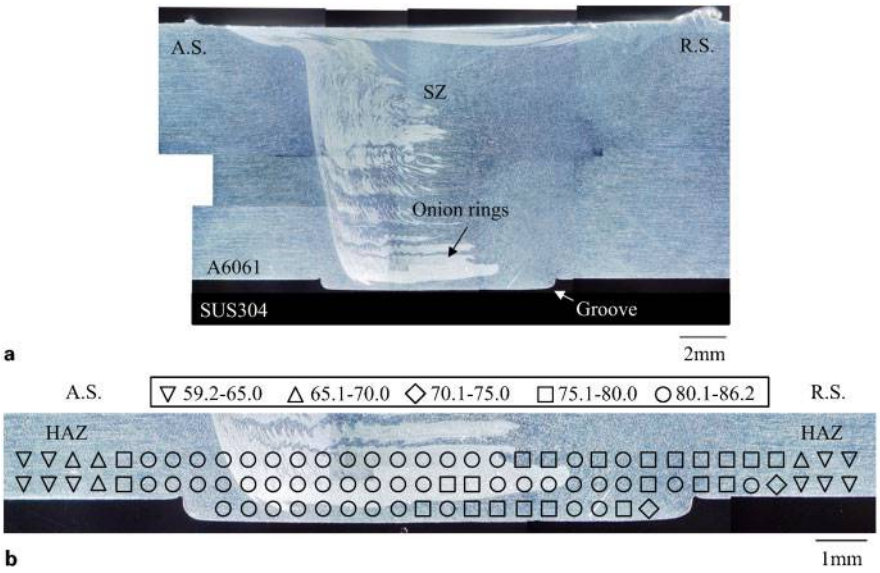


**2** ***a*** **stereomicroscope image of interface of friction stir welded A6061/SUS 304 grooved lap joint and** ***b*** **hardness distribution at bottom of A6061 plate**

region in the specimen used in this study. The negative and positive distances from the centre of the tool represent the advancing and retreating sides respectively. It was found that the specimen could not be prepared in the region beyond 2·75 mm from the centre because of the occurrence of an interfacial fracture during wire cutting. The bonded area at the interface was $\sim 7{\cdot}6$ mm$^2$ (the square of 2·75 mm). This implies that $\sim 62\%$ of the area along which the rotating tool passed the specimen was regarded as the bonded region (the square of the tool radius is $\sim 12{\cdot}3$ mm$^2$). Within this bonded region, the distribution of the maximum tensile strength was 194–212 MPa, except in the case of the specimen cut from 0·25 mm (maximum tensile strength: 243 MPa); this value is around the same as that of the base alloy ($212 \pm 10$ MPa). In all the investigated specimens, it was observed that fracture occurred at the A6061 matrix, and not on the interface of the joint. Figure 4 shows a typical specimen fractured at the A6061 matrix (cut from 0·5 mm at the advancing side). The fractured region shows necking and dynamic recrystallisation of A6061. On the other hand, from the magnified image of the interface shown in Fig. 4*b*, it seems that there are no metallurgical change at the interface, indicating that the interface will not deform during the microtensile test.

The deformation behaviour of the joint was examined from the corresponding stress–strain curve obtained during the microtensile test. Figure 5 shows the obtained stress–strain curve of the joint cut from 0·5 mm at the advancing side. For the sake of comparison, the stress–strain curve of the A6061 base alloy is also shown. The joint showed longer elongation (strain), which was contributed to the deformation of A6061. Moreover, it should be noted that although the maximum strength of

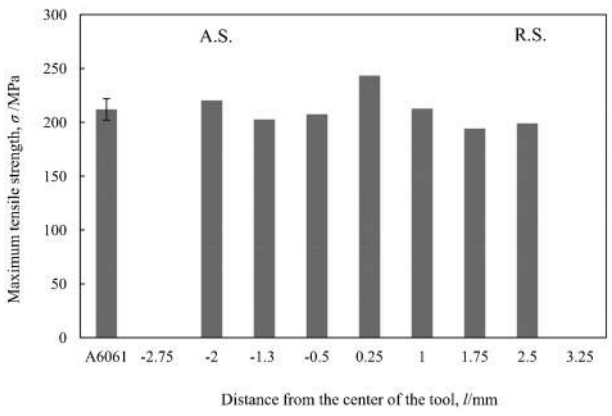


**3 Maximum tensile strength of friction stir welded A6061/SUS 304 grooved lap joint, obtained from microtensile test**

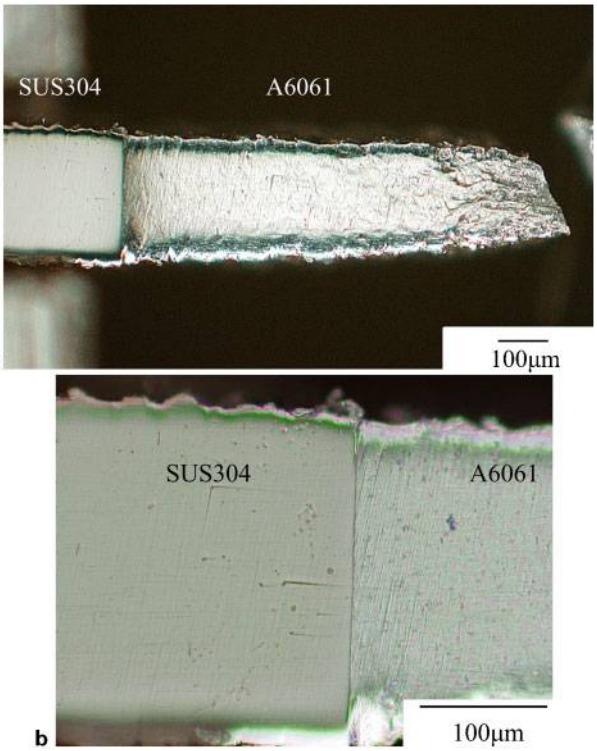


**4** ***a*** **specimen fractured at A6061 matrix after microtensile test (cut from 0·5 mm at advancing side) and** ***b*** **magnified image of interface in friction stir welded A6061/SUS 304 grooved lap joint**

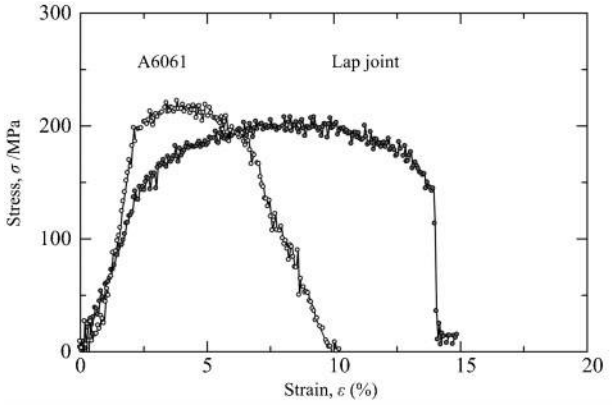


**5 Stress–strain curves of friction stir welded A6061/SUS 304 grooved lap joint (cut from 0·5 mm at advancing side) for microtensile test and A6061 base alloy**

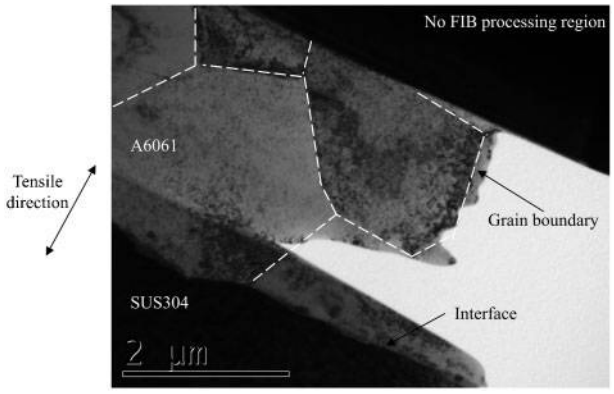


**6 Image (TEM) of interface of friction stir welded A6061/SUS 304 grooved lap joint (cut from 0·5 mm at advancing side) after occurrence of fracture**

the joint was approximately the same as that of the A6061 base alloy, the proof stress of the joint decreased to ~80% that of the base alloy.

The microtensile test revealed that ~62% of the area along which the rotating tool passed the specimen was regarded as the bonded region. A fracture occurred not at the interface of the joint but at the A6061 matrix within the area. The maximum tensile strength of the joint was approximately the same as that of the base alloy; however, the proof stress of the joint decreased to ~80% that of the base alloy. Transmission electron microscopy observation was carried out to precisely investigate the interfacial microstructures of the specimen after the occurrence of a fracture. The sample used for the TEM observation was directly prepared from the joint after the occurrence of a fracture, using FIB. Figure 6 shows the TEM image of the interface of the joint. The white broken lines shown on this figure are the grain boundaries of the A6061 matrix. It should be noted that the grains were equiaxed and not elongated along the tensile direction. This observation proves that the interface deformed only slightly during the tensile test.

Figure 7 shows the scanning transmission electron microscopy–EDX mapping at the interface of the joint. This figure confirms the presence of two types of interfacial microstructures, namely, microstructures made of an oxide and an intermetallic compound; this figure also shows that some elements composed of the base alloys were enriched within the microstructures. Figure 8 and Table 2 show the selected area electron diffraction (SAED) pattern and the quantified EDX results. From the SAED pattern, the oxide and intermetallic compounds were identified to be $Al_2O_3$ and $Al_8Fe_2Si$ respectively. Although further investigation on the formation mechanism of the layers made of these compounds is required, at present, it is considered that the fracture of the sound joint at the A6061 matrix was attributed to the formation of very thin interfacial reaction layers.

Localised frictional heating during FSW brings about microstructural changes, particularly changes such as precipitation distribution.[22] As a result of the extensive studies conducted on the precipitation process of the Al–Mg–Si alloy system,[23–27] the following precipitation sequence has now been generally accepted:

Super saturated solidsolution $\alpha \rightarrow$nanoscale clusters,

G. P. zone$\rightarrow\beta''\rightarrow\beta'\rightarrow\beta$ ($Mg_2Si$)

It is well known that the fine and dense distribution of the needle shaped $\beta''$ phase greatly contributes to the strength of this alloy system. Figure 9*a* shows a typical $\beta''$ phase of the Al–0·83Mg–0·51Si (mass-%) ternary alloy aged at 443 K for 86·4 ks, which is the condition under which this alloy shows maximum hardness. Figure 9*b* shows the A6061 matrix near the interface shown in Fig. 6. The dense defect and dislocation loop result from beam damages caused by the FIB process, which are inevitable to prepare a sample for TEM using FIB. Contrary to that shown in Fig. 9*a*, the $\beta''$ phase could not be seen in the matrix; moreover, the SAED patterns did not show the streaks of the $\beta''$ phase along $[100]_{Al}$, indicating that the $\beta''$ phase formed during the T6 process (solution heat treated and then artificially aged) was dissolved during FSW. Although the exact temperature of the interface during FSW cannot be estimated because of the lack of experimental data, the peak temperature of the interface of an aluminium alloy/steel dissimilar joint during FSW seems to be higher than that of friction stir welded 6061 Al-T6 plates (~723 K);[10] this temperature is considerably higher than that of the dissolution of the $\beta''$ phase (below 675 K).[22] The dissolution of the $\beta''$ phase during FSW well corresponds to the results of mechanical properties, i.e. a decrease in the hardness (Fig. 2) and proof stress (Fig. 5) of the joint. Therefore, it can be concluded that in the FSW process of an age hardenable alloy, the maximum strength of the alloy was obtained to be approximately the same as that of the base metal, and fracture occurred in the base metal owing to the formation of very thin interfacial reaction layers. However, it should also be pointed out that the proof stress of the joint decreases, indicating that it is easy to deform the joint through the dissolution of the $\beta''$ phase under heat.

## Conclusions

1. Approximately 62% of the area along which the rotating tool passed the specimen was regarded as the bonded region and the sound joint fractured at the A6061 matrix within this region.

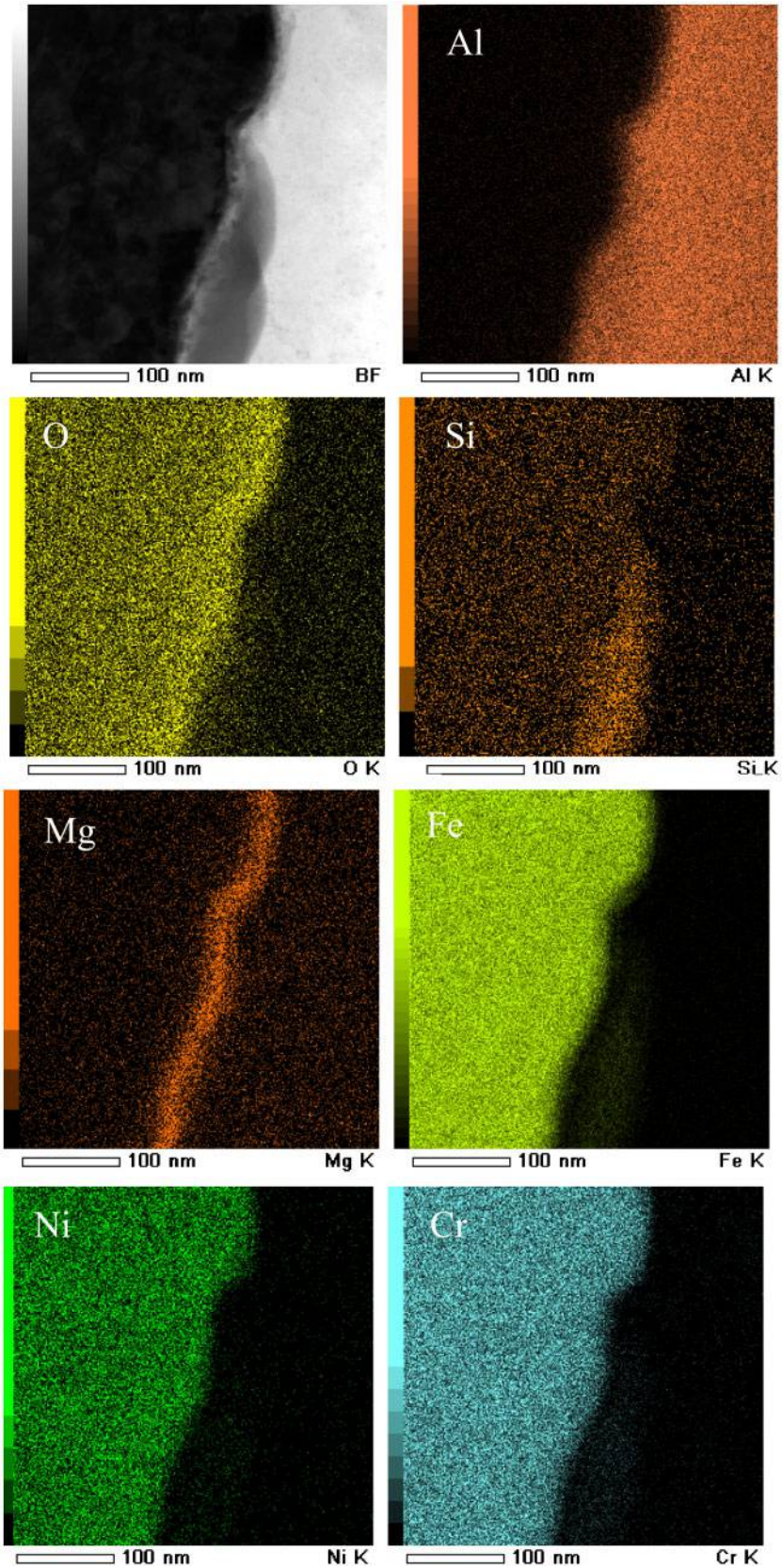


**7 Scanning transmission electron microscopy–EDX mapping at interface of friction stir welded A6061/SUS 304 grooved lap joint (cut from 0·5 mm at advancing side)**

2. The fracture of the sound joint at the A6061 matrix was attributed to the formation of very thin interfacial reaction layers ($Al_2O_3$ and $Al_8Fe_2Si$).

3. Equiaxed aluminium grains were observed at the interface of the specimen after it was fractured, clearly indicating that the interface deformed only slightly during the microtensile test.

4. It is important to note that although the maximum tensile strength of the joint was approximately the same as that of the base alloy, the proof stress of the joint

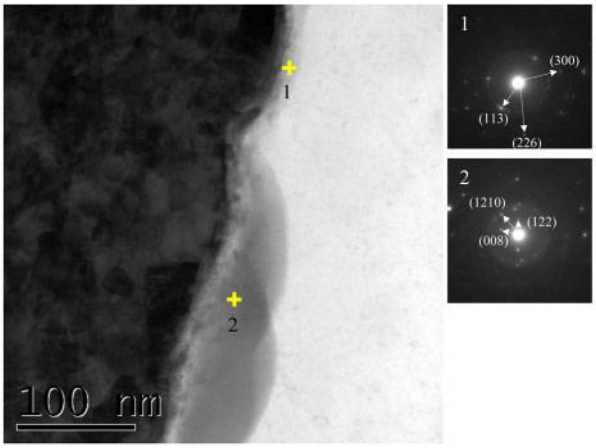


**8 Selected area electron diffraction patterns of interfacial microstructures in A6061/SUS 304 grooved lap joint (cut from 0·5 mm at advancing side)**

**Table 2 Material compositions within interfacial microstructures of friction stir welded A6061/SUS 304 grooved lap joint, as determined by EDX analysis/mol.-%**

| Points | O | Mg | Al | Si | Cr | Fe | Ni |
|---|---|---|---|---|---|---|---|
| 1 | 35·3 | 1·8 | 44·0 | 2·0 | 2·6 | 4·4 | None |
| 2 | 5·9 | None | 68·1 | 7·5 | 3·1 | 15·0 | 0·4 |

decreased to ~80% that of the base alloy. This is because the generation of heat during FSW dissolved the $\beta''$ phase in the A6061 aluminium alloy.

## Acknowledgements

The authors would like to thank Professor M. Takahashi of Osaka University and Professor T. Shibayanagi of Osaka University (now Toyama University) for their significant help with the TEM observation. A part of this work was conducted under the Cooperative Research Program of Institute for Joining and Welding Research Institute, Osaka University. This study was financially supported by the Japan Aluminium Association, Suzuki Foundation and Priority Assistance for the Formation of Worldwide Renowned Centers of Research – The Global COE Program (Project: Center of Excellence for Advanced Structural and Functional Materials Design) from the Ministry of Education, Culture, Sports, Science and Technology (MEXT), Japan.

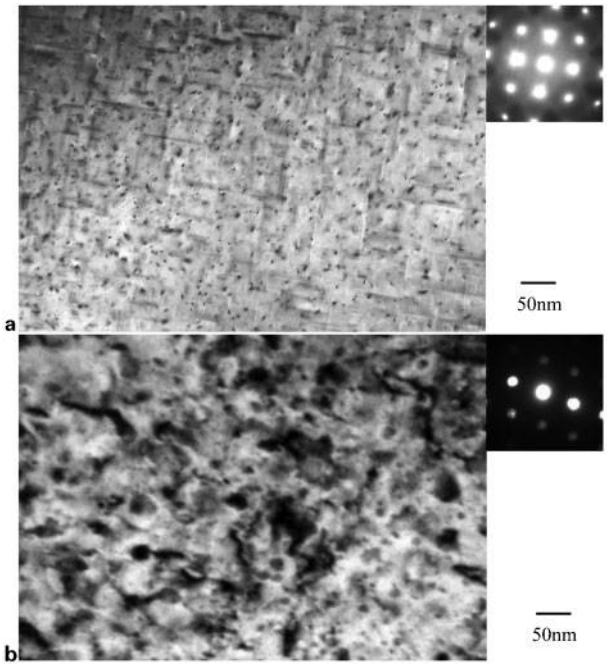


**9 Images (TEM) of *a* Al–0·83Mg–0·51Si (mass-%) ternary alloy aged at 443 K for 86·4 ks and *b* A6061 matrix near interface shown in Fig. 6**

## References

1. M. Roulin, J. W. Luster, G. Karadeniz and A. Mortensen: *Weld. J.*, 1999, **78**, 151–155.
2. E. Schbert, M. Klassen, I. Zener, C. Walz and G. Sepold: *J. Mater. Process. Technol.*, 2001, **115**, 2–8.
3. H. T. Lee and M. H. Chen: *Mater. Sci. Eng.*, 2002, **333**, 24–34.
4. K. J. Lee and S. Kumai: *Mater. Trans.*, 2006, **47**, 1178–1185.
5. R. Padmanabhan, M. C. Oliveira and L. F. Menezes: *Mater. Des.*, 2008, **29**, 154–160.
6. T. Ogura, H. Umeshita, Y. Saito and A. Hirose: *Q. J. Jpn Weld. Soc.*, 2009, **27**, 174–178.
7. T. Ogura, K. Ueda, Y. Saito and A. Hirose: *Mater. Trans.*, 2011, **52**, 979–984.
8. W. M. Thomas, E. D. Nicholas, J. C. Needham, M. G. Church, P. Templesmith and C. Dawes: International Patent Application no. PCT/GB92/02203 and GB Patent Application no. 9125978·9, 1991.
9. T. Ogura, Y. Saito, T. Nishida, H. Nishida, T. Yoshida, N. Omichi, M. Fujimoto and A. Hirose: *Scr. Mater.*, 2012, **66**, 531–534.
10. R. S. Mishra and Z. Y. Ma: *Mater. Sci. Eng. R*, 2005, **R50**, 1–78.
11. T. Watanabe, A. Yanagisawa and H. Takayama: *Q. J. Jpn Weld. Soc.*, 2004, **22**, 141–148.
12. C. M. Chen and R. Kovacevic: *Int. J. Mach. Tools Manufact.*, 2004, **44**, 1205–1214.
13. A. Elrefaey, M. Takahashi and K. Ikeuchi: *Q. J. Jpn Weld. Soc.*, 2005, **23**, 186–193.
14. W. B. Lee, M. Schmuecker, U. A. Mercardo, G. Biallas and S. B. Jung: *Scr. Mater.*, 2006, **55**, 355–358.
15. Y. C. Chen, T. Komazaki, T. Tsumura and K. Nakata: *Mater. Sci. Technol.*, 2008, **24**, 33–39.
16. K. Miyagawa, M. Tsubaki, T. Yasui and M. Fukumoto: *Q. J. Jpn Weld. Soc.*, 2008, **26**, 131–136.
17. R. S. Coelho, A. Kostka, S. Sheiki, J. dos Santos and A. R. Pyzalla: *Adv. Eng. Mater.*, 2008, **10**, 961–972.
18. T. Tanaka, T. Morishige and T. Hirata: *Scr. Mater.*, 2009, **61**, 756–759.
19. T. Nishida, T. Ogura, H. Nishida, T. Yoshida, N. Omichi, M. Fujimoto and A. Hirose: Preprints of the National Meeting of JWS, 2011, **89**, 122–123.
20. A. Arora, Z. Zhang, A. De and T. Debroy: *Scr. Mater.*, 2009, **61**, 863–866.
21. R. Nandan, G. G. Roy, T. J. Lienert and T. Debroy: *Acta Mater.*, 2007, **55**, 883–895.
22. Y. S. Sato, H. Kokawa, M. Enomoto and S. Jogan: *Metall. Mater. Trans. A*, 1999, **30A**, 2429–2437.
23. G. Thomas: *J. Inst. Met.*, 1961–1962, **90**, 57–63.
24. A. Kelley and R. B. Nicholson: *Prog. Mater. Sci.*, 1963, **10**, 151–391.
25. K. Matsuda and S. Ikeno: *J. Jpn Inst. Light Met.*, 2000, **50**, 23–36.
26. A. K. Gupta, D. J. Lloyd and S. A. Court: *Mater. Sci. Eng. A*, 2001, **A316**, 11–17.
27. T. Sato: *J. Jpn Inst. Light Met.*, 2006, **56**, 592–601.